17th World Conference on Earthquake Engineering, 17WCEE
Sendai, Japan - September 13th to 18th 2020

Reverse Cyclic Behaviour of Concrete Shear Walls Reinforced with High-Strength Steel Reinforcement

N. Aghniaey[(1)], M. Saatcioglu[(2)], H. Aoude[(3)]

[(1)] *Ph.D. Candidate, University of Ottawa, naghn087@uottawa.ca*
[(2)] *Distinguished University Professor, University of Ottawa, Murat.Saatcioglu@uottawa.ca*
[(3)] *Associate Professor, University of Ottawa, Hassan.Aoude@uottawa.ca*

Abstract

Structural walls, more commonly known as shear walls are widely used as part of the seismic force resisting systems in concrete buildings. Such walls are ordinarily reinforced with conventional steel reinforcement that have a maximum specified yield strength of 400 MPa. The American concrete code ACI 318 [1] limits design yield strength of reinforcement in seismic applications to 400 MPa with few exceptions. Similarly, the Canadian Concrete Design Code CSA A23.3 [4] discourages the use of reinforcement with specified yield strengths of higher than 400 MPa in seismic applications. The use of higher strength reinforcement in such walls may be advantageous in reducing reinforcement congestion and improving constructability. However, data on the seismic behavior of structural walls built with higher strength steel reinforcement is limited, particularly in the case of concrete shear walls reinforced with Grade 690 MPa steel. To help provide much needed data, a concrete shear wall reinforced with Grade 690 MPa ASTM A1035 reinforcement was constructed and tested under constant axial compression and cyclic load reversals. The wall was geometrically identical to a concrete shear wall reinforced with conventional flexural reinforcement that had been previously tested at the University of Ottawa. The wall tested in the current investigation was a ¼ -scale representation of a 6-storey shear wall with a height-to-length aspect ratio of 3.0. Test results show that a drift capacity (Δ/H) of 2.0% was reached prior to failure of the wall due to rupture of the longitudinal reinforcement. The ductility of the wall was approximately 30% less than that of the previously tested wall reinforced with Grade 400 MPa reinforcement. The wall exhibited a flexural behaviour as expected, and sustained only minor concrete damage throughout the test. It was noted that the wall reached the same moment capacity compared to the control wall with ordinary Grade 400 MPa reinforcement with approximately 36% less flexural reinforcement in the boundary elements. VecTor2 Finite Element Modeling software was used to model the wall. A parametric study was conducted using VecTor2 software to investigate the impact of selected design parameters on its seismic behaviour. These parameters included aspect ratio (H/L) and reinforcement type. Analytical results show that the reinforcement grade has a significant impact on ductility, energy dissipation capacity, and general behavior of the wall. The analytical results also show that wall aspect ratio has a pronounced effect on the behaviour of the shear wall considered.

Keywords: High-Strength, Steel, Concrete, Shear Wall, Seismic

1. Introduction

Concrete shear walls are ordinarily reinforced with conventional steel reinforcement that have a maximum specified yield strength of 400 MPa. Recent advancements in steel manufacturing technology have led to the development of High-Strength Steel (HSS) reinforcement with yield strengths of 550 MPa and greater, and interest in their use in concrete construction has been steadily growing. One of the potential applications of HSS bars is in the shear walls of concrete buildings, where their use can allow for reduced reinforcement congestion, improved constructability and reduced cost. The US National Institute of Standards and Technology (NIST) conducted case studies of two high-rise buildings with shear wall and moment frame seismic force resisting systems. Despite a 5% premium for the higher grade reinforcement, replacing conventional steel with HSS reinforcement was found to reduce overall structural costs by 3.4% and 3.8% for the shear wall and moment frame buildings, respectively [8].

On the other hand, current concrete design guidelines only allow limited use of high-strength reinforcement in concrete construction, especially in seismic applications. For example, the Canadian CSA A23.3 standard [4] discourages the use of HSS reinforcement in seismic concrete members and states that the "additional strains required for higher yield-strength steel will generally reduce ductility". Similarly, the ACI 318 code [1] limits the yield strength of reinforcement used in earthquake-resistant construction, with few exceptions. Use of high-strength reinforcement in seismic structures is limited due to their potential impact on ductility of structural concrete members. In particular, most high-strength steels have a different stress-strain behaviour compared to the conventional steel, with reduced strain capacity and lack of a well-defined yield point or yield plateau. While extensive studies have examined the seismic response of high-strength steel reinforced concrete (HSS-RC) columns [12], information on the strength and ductility of HSS-RC walls is limited, particularly in the case of walls with higher aspect ratios. Similarly, most of the existing research have focused on walls reinforced with Grades 500 MPa to 550 MPa bars. Data on experimental investigation involving walls with Grade 690 MPa reinforcement (that have unconventional stress-strain behaviour) is limited.

A limited number of studies have focused on HSS-RC walls. Previous tests include concrete shear walls with aspect ratios ranging from 1 to 3 and flexural reinforcement with yield strengths of 530 MPa to 770 MPa that conform to different reinforcing steel standards. Some studies suggest that the ductility of concrete shear walls reinforced with high-strength reinforcement is low if the steel lacks a well-defined yield point or plateau [3, 5]. Based on the available data, this reduction is generally more pronounced in walls with higher aspect ratios where wall response is flexure-dominant. Other studies with walls reinforced with steel conforming to ASTM A615, which generally exhibits a well-defined yield point and yield plateau reported that high-strength reinforcement did not have a significant impact on ductility of the walls [2, 12]. Dazio [5] shows that the plastic hinge behavior of such shear walls are impacted by high-strength steel reinforcement that lack a defined yield point or a yield plateau.

This study aims at increasing the understanding of the seismic behavior of slender concrete walls built with higher strength reinforcement. The scope of the overall project includes combined experimental and analytical research involving ¼-scale concrete shear walls with aspect ratios of 2.0 and 3.0, reinforced with Grade 690 MPa steel subjected to cyclic load reversals and constant axial load. The current paper presents the results of wall W-2HS with an aspect ratio (H/L) of 3.0. An analytical study is included to evaluate the response of the tested wall using Finite Element Modelling (FEM). A parametric study, utilizing VecTor2 software, is also included to assess the effects of wall aspect-ratio and steel type on wall behaviour.

2. Experimental Investigation

2.1 Objectives

There is lack of experimental research data on the behaviour of HSS-RC walls with high-strength steel grades that do not exhibit a well-defined yield point or yield plateau. A ¼-scale concrete shear wall, labelled W-2HS, with an aspect ratio of 3.0 and a steel Grade of 690 MPa, conforming ASTM A1035, was constructed and tested under cyclic load reversals in an effort to fill the existing research gaps. The objective was to investigate the effect of such high-strength reinforcement on strength, ductility and energy dissipation capacity of reinforced concrete shear walls.

2.1 Tested Wall Details

Wall W-2HS was a ¼-scale specimen representing a shear wall of a 6-story building designed to be a "ductile wall" as per CSA A23.3-14 [4]. The wall was 4330 mm high at the lateral loading point and 1450mm long, having an aspect ratio of 3.0. It can be considered a slender wall and was designed to exhibit a flexure-dominant response. It had a barbell-shaped cross-section with 250mmx250mm square boundary elements and a 100mm thick web section. The base of the wall was monolithically attached to a heavily-reinforced concrete foundation which was used to anchor the base of the wall to the laboratory strong floor. The wall was initially designed in accordance with ACI 318-14 [1] and was modified to conform to the requirements of CSA A23.3-14 [4]. The geometry of the wall was identical to a wall previously tested at the University of Ottawa by Navidpour [10] with conventional Grade 400 MPa flexural and web reinforcement conforming to ASTM A615. Flexural reinforcement ratio of wall W-2HS was reduced in proportion to the ratio of its tensile strength to that of the conventional Grade 400 MPa reinforcement to achieve a similar probable moment capacity to that of the wall tested by Navidpour [10] to facilitate direct comparison.

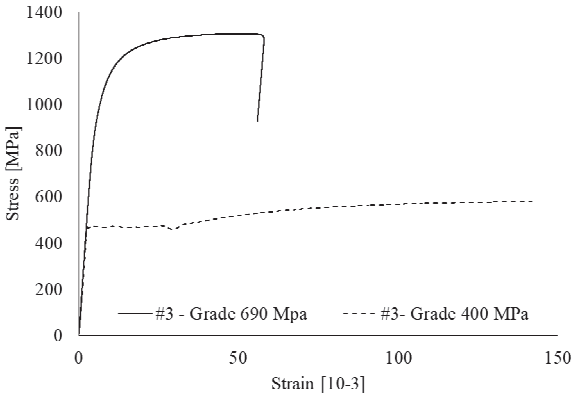

Fig. 1 -Typical Stress-Strain Diagram for no. 3 Grade 690 MPa ASTAM A1035 Steel compared to conventional 400 MPa ASTM 615 Steel

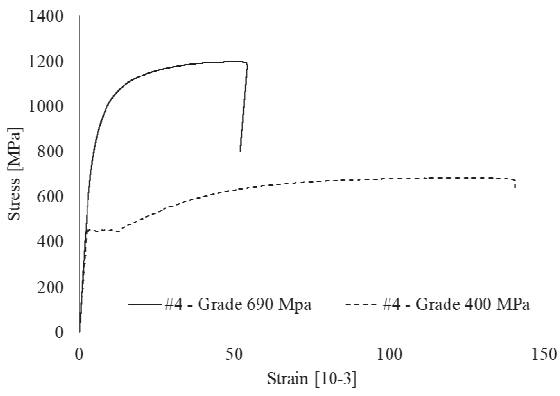

Fig. 2 -Typical Stress-Strain Diagram for no. 4 Grade 690 MPa ASTAM A1035 Steel compared to conventional 400 MPa ASTM 615 Steel

The boundary element longitudinal reinforcement consisted of 12 equally spaced No. 4 bars (12.7mm dia.) confined with No. 3 (9.525mm dia.) bars spaced at 75mm c/c. The web reinforcement consisted of No. 3 vertical and transverse reinforcement at 300mm and 200mm spacings, respectively. In all cases the reinforcement consisted of Grade 690 MPa steel conforming to ASTM A1035. The concrete used to construct the wall was designed and mixed in-house with a target 28-day compressive strength of 80 MPa. The average compressive strength of concrete on the day of testing, as determined from compression testing of 100 mm × 200 mm cylinders, was 84 MPa. The properties of the high-strength reinforcement were obtained based on tensile tests on three random specimens for each bar size. Using the 0.2% offset method, the average yield strengths of the No. 3 and No.4 bars were determined to be 900 MPa and 928 MPa (typical stress-strain curves are shown in Fig. 1 and Fig. 2).

2.1 Loading and Instrumentation

Loading consisted of cyclic lateral load reversals and constant axial load equivalent to 8% of wall's concentric axial capacity. The lateral load was applied using a 1000kN MTS actuator attached to a rigid steel frame as shown in Fig. 3. Applied lateral load was measured via a load cell built into the MTS actuator. Axial load was applied using 10 post-tensioned 7-wire strands as prestressing cables. Special anchors were previously designed and built at the University of Ottawa to attach the post-tensioning cables to the foundation. The correlation between the axial forces and strains of the post-tensioning cables were previously established and was used to monitor axial tension during the initial loading, as well as during the wall test to determine variation of wall axial load at different stages of testing.

As ASTM A1035 reinforcing bars do not have a defined yield point, it is difficult to pinpoint a specific yield displacement that is typically used in developing cyclic loading protocols. In order to ensure that the yield point of the wall was effectively captured during testing, small initial drift increments of 0.2% were applied up to a lateral drift of 1.0%. The size of the increments was selected based on the predicted yield 'region' of the wall that was obtained analytically using VeTor2 Finite Element Modelling software. Once yielding of the wall was confirmed, lateral cyclic displacements continued at increments of 0.5% drift ratio up to failure.

Displacement transducers were installed at critical locations of the wall, as shown in Fig. 4, to record lateral deflections as well as shear deformations in the web section. Cable transducers were also installed at the wall base (30mm above the wall base) to record wall deflections due to anchorage slip (extension of reinforcement in the foundation). Strains in the steel reinforcement were measured using TML 120Ω strain gauges attached directly onto the bars at locations of interest, as shown in Fig. 4, which included the outermost boundary element longitudinal reinforcement, as well as the web transverse reinforcement within the plastic hinge region of the wall.

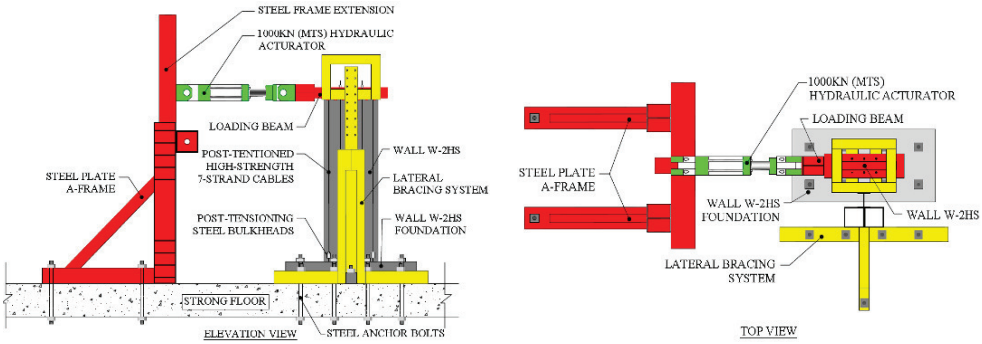

Fig. 3 – Loading Setup

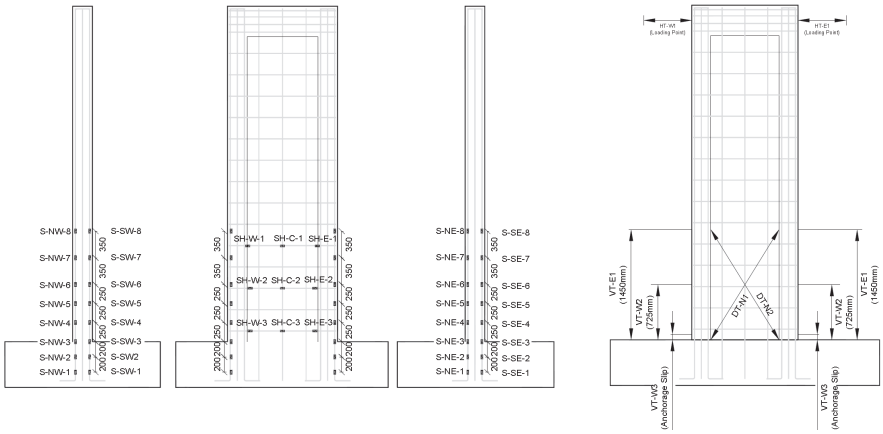

Fig. 4 - Wall W-2HS Instrumentation Plan

2.1 Test Observations

The very first loading cycle generated horizontal flexural cracks in the boundary elements, which propagated diagonally into the web. More cracks appeared during subsequent load stages. However, the crack widths did not increase appreciably throughout the test except for a single large crack that formed at the base of the wall, which widened under increased deformation reversals until failure. Diagonal crack widths remained small throughout the test, which suggested that shear deformations were small as expected, and that shear was effectively controlled in the web. No sign of buckling in the longitudinal reinforcement was observed. No major damage occurred until the longitudinal bars started to rupture during the first cycle at 2.0% drift. The wall sustained minimal concrete damage throughout the test. Fig. 5 shows photos of the marked cracks at yield and following the rupture of first reinforcing bar. It can be seen that very few new cracks appeared between the initial yield and the wall failure. Loss of cover due to concrete spalling started at 1.5% drift ratio, and was limited to the outer faces of the boundary elements within the bottom 150mm wall segment. Confined concrete within the core of the boundary elements remained intact throughout the test.

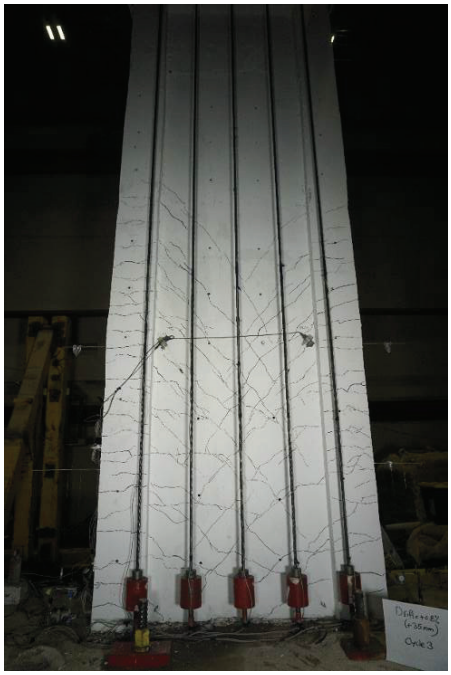

a) Wall2-HS at yield

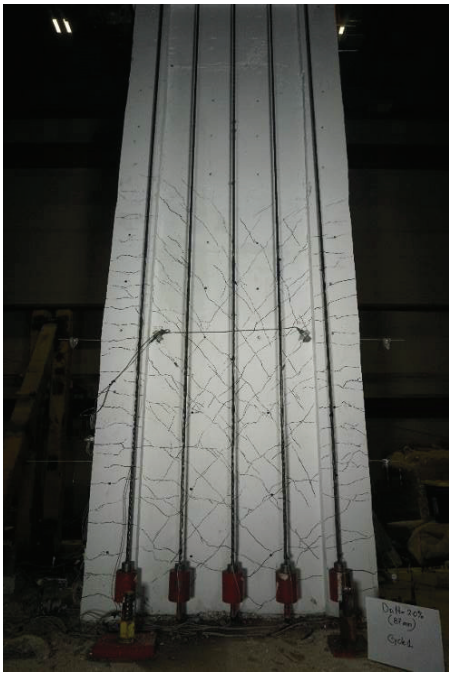

b) Wall2-HS at first bar rupture

c) Extent of damage on the east side boundary element at the end of test

d) Extent of damage on the west side boundary element at the end of test

Fig. 5 - Wall W-2HS at Yield and at First Bar Rupture

2.1 Results and Discussion

Fig. 6 illustrates the hysteretic response of wall W-2HS. Table 1 shows measured test parameters at different loading stages up to the rupture of flexural reinforcement. In general, wall W-2HS exhibited the characteristics of a flexural shear wall and failed in flexure due to the rupture of longitudinal reinforcement in the boundary elements. The first longitudinal reinforcing bar ruptured in the positive direction at a lateral displacement of 87mm (2.0% drift) and applied lateral load of 592 kN (M_u = 2563 kN.m). This occurred during the first cycle of the 2.0% drift stage. More bars ruptured during the second cycle of the same deformation level in the positive direction. It was difficult to visually determine the exact number of ruptured bars at this stage of testing. However, FEM analysis of the wall suggested that three outer longitudinal bars likely ruptured at this stage. Following the second cycle of the 2.0% drift stage, loading was reversed, and cyclic load reversals continued in the negative direction. Additional bars ruptured in the negative direction during the third cycle of 2.5% drift stage, at which point the capacity of the wall reduced to approximately 50% of the ultimate load and the test was stopped.

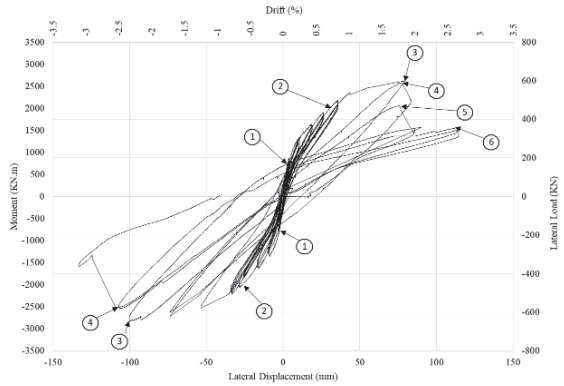

Fig. 6 – Wall W-2HS Hysteresis Diagram

(1) first crack; (2) yield; (3) maximum load; (4) first bar rupture; (5) second bar rupture; (6) additional cycles in the positive loading direction following bar ruptures

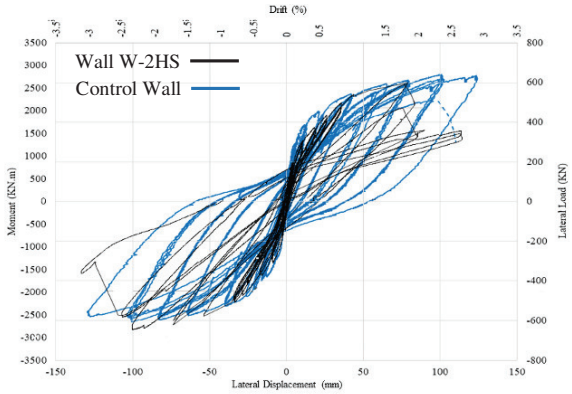

Fig. 7 – Comparison of hysteresis diagrams for Wall W-2HS and Control Wall (Wall 3 by Navidpour[10])

Table 1 – Wall W-2HS Experimental Results

Loading Stage	Positive Loading						Negative Loading					
	F (KN)	M (KN.m)	Δ_{top} (mm)	Δ_p (mm)	Δ_{sh} (mm)	Drift (%)	F (KN)	M_r (KN.m)	Δ_{top} (mm)	Δ_p (mm)	Δ_{sh} (mm)	Drift (%)
Cracking	188.1	814.5	9.1	0.1	-0.1	0.21	203.1	879.4	10.1	0.1	-0.4	0.23
0.4 Yield	292.5	1266.3	15.7	3.1	0.0	0.36	257.1	1113.2	13.3	1.4	-0.1	0.31
0.8 Yield	405.1	1754.3	31.0	10.3	-0.1	0.72	362.5	1569.6	26.6	9.1	0.5	0.61
Yield	451.4	1954.6	38.7	13.1	-0.1	0.89	431.4	1867.8	33.2	13.9	1.0	0.77
1.4 Yield	539.2	2334.7	54.3	22.8	2.2	1.25	502.6	2176.2	46.6	23.2	2.6	1.08
1.8 Yield	602.6	2609.3	69.8	34.7	2.3	1.61	579.0	2506.9	59.8	31.0	2.3	1.38
2.0 Yield	632.2	2737.2	77.7	43.2	2.2	1.79	597.0	2585.0	66.7	41.4	3.3	1.54
Load	625.5	2708.3	89.2	56.1	2.3	2.06	645.9	2796.7	77.6	48.6	-	1.79
Rupture	591.5	2561.3	87.0	59.4	2.2	2.01	646.0	2797.1	109.8	73.4	-	2.54

F=top lateral force; **M** = moment; Δ_{top} = total top displacement; Δ_p = top displacement due to rotation within plastic hinge region (1450mm from wall base); Δ_{sh} = top displacement due to shear

Fig. 7 compares the experimental results for wall W-2HS and the control wall tested by Navidpor[10]. Both walls had similar flexural load capacities as intended. Wall W-2HS behaves very similarly to Navispour's wall up to a drift ratio of about 1.5%, matching its initial stiffness up to the cracking point and the general shape of the backbone curve. It is noted that wall W-2HS exhibits reduced stiffness between cracking and the

onset of yield. It is also observed that the unloading branches of Navispour's wall are wider compared to wall W-2HS, resulting in higher energy dissipation capacity. In other words, wall W-2HS exhibits more 'pinching'. This is attributed to the yield behaviour of high-strength reinforcing steel. Conventional ASTM A615 steel has a defined yield point beyond which the reinforcing steel becomes fully plastic while the ASTM A11035 steel has a 'yielding region' within which it exhibits partially elastic behaviour in a larger tensile strain range. This leads to self-centering action by the reinforcement, which pulls the wall back to its original position as it restores its elastic deformation within the partial yielding region.

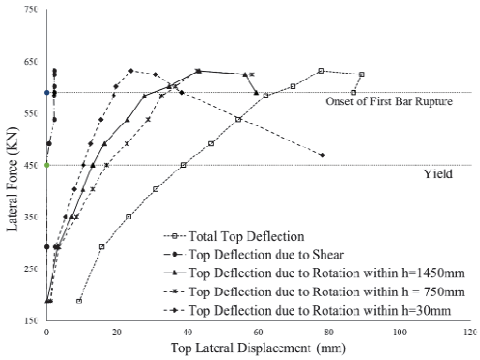

a) Force-Displacement Diagrams for Loading in Positive Direction

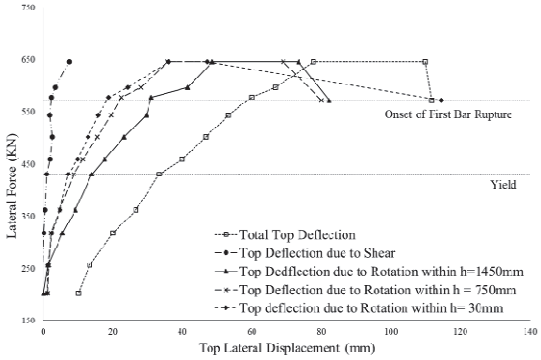

b) Force-Displacement Diagrams for Loading in Negative Direction

Fig. 8 - Force-Displacement Diagrams for Positive and Negative Loading Directions

Using the data recorded by the cable transducers, rotations of the wall at different elevations along the height of the wall were translated to top lateral deflections. Fig. 8a) and b) show backbone force-displacement curves resulting from the rotations recorded at different elevations along the height of the wall for positive and negative load directions, respectively. Recorded shear displacements as well as total top lateral deflection of the wall are also shown. Fig. 8 suggests that a large proportion of the rotation within the plastic hinge region occurs within about 30mm of the base of the wall. Approximately 70% of the plastic hinge rotation at the onset of the first flexural bar rupture in the positive direction is due to the rotation of the wall within the 30mm wall segment at the base. Similarly, this ratio is 65% in the negative direction. Furthermore, the ratio of the contribution of rotation within the plastic hinge region to the total top displacement is only 15% prior to cracking. This contribution increases to 39% at yield, 54% at ultimate load and 67% at first bar rupture. This assessment is in agreement with the cracking behavior observed during testing. Most cracks above the base of the wall maintained small widths throughout the test where one major crack at the wall-foundation interface continued to widen until the wall failure. In summary, despite similar flexural capacities, it can be observed that wall W-2HS fails due to the rupture of reinforcement at a drift level of about 2.0% whereas its companion wall with Grade 400 MPa steel continues for another 0.8% drift before failure. This is a 29% reduction in ductility of the wall which can be attributed to the use of less ductile high-strength reinforcement.

Strains along the boundary element longitudinal reinforcement were recorded using strain gauges installed at 250mm and 350mm intervals within the plastic hinge region (refer to Fig. 4). Fig. 9a) and b) show the strains in the outermost reinforcing bars in positive and negative loading directions respectively. It can be observed that steel strains increase rapidly at the base of the wall closer to the ultimate load, which suggests that plastic hinging is mostly limited to the very base of the wall. Fig. 9 c) and d) show strains in the outermost longitudinal reinforcement plotted against lateral forces in the positive and negative loading directions. It can be observed that the longitudinal bars become plastic and continue to strain until failure at the base of the wall. Recorded strains at the strain gauge level above (250mm above wall base) are significantly lower.

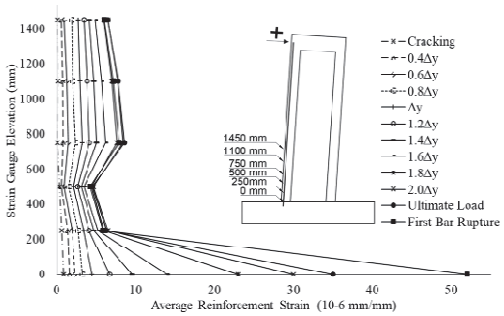

a) Steel Strains vs wall height in Positive Loading Direction

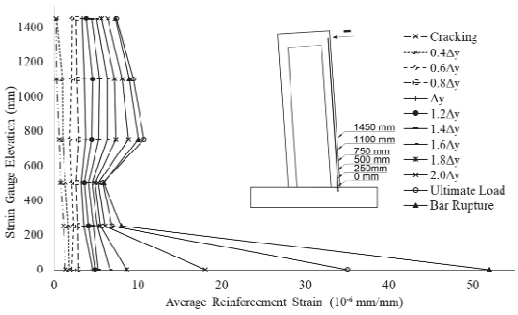

b) Steel Strains vs wall height in Negative Loading Direction

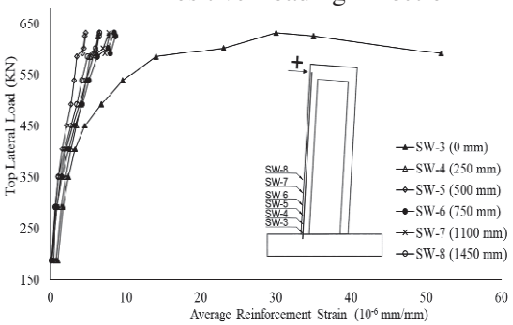

c) Steel Strains vs Lateral Force in Positive Loading Direction

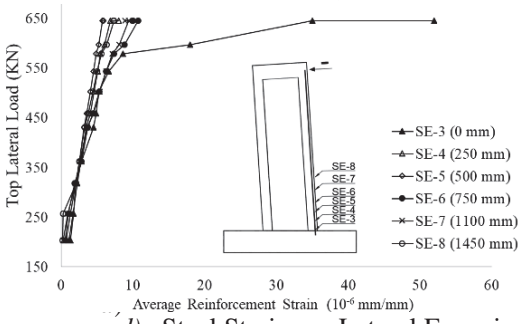

d) Steel Strains vs Lateral Force in Negative Loading Direction

Fig. 9 – Wall W-2HS Steel Strains Plotted against Lateral Load and Wall Height

2. Analytical Investigation

Finite Element Modeling (FEM) of the wall specimen was performed using a specialized FEM software called VecTor2, developed based on the Modified Compression Field Theory for nonlinear finite element analysis of reinforced concrete members subjected to in-plane, normal, and shear stresses. The program has been under development since 1990 at the University of Toronto and has been used extensively to model the behavior of reinforced concrete walls. A comprehensive software verification was conducted as part of this study using the data obtained from previous experimental investigations conducted by other researchers [8, 5, 6]. It was found that VecTor2 can effectively and accurately predict the reverse cyclic behavior of concrete shear walls within a wide range of properties, including different wall aspect ratios, steel types, and concrete strengths.

Fig. 10a) shows the meshed FEM model used in the VecTor2 analysis of wall W-2HS. Four regions were defined to model the wall: 1) foundation, 2) web section, 3) boundary elements, and 4) lateral loading region. Each region was defined based on its corresponding thickness and reinforcement ratio. Hybrid rectangular mesh with a maximum mesh size of 100mm, and a maximum aspect ratio of 1.5 was used to discretize the wall. Longitudinal reinforcement within the boundary elements and the web section were defined as individual steel trusses with assumed perfect bond to the adjoining concrete elements. Transverse reinforcement was defined by reinforcement ratio as 'smeared' reinforcement in the horizontal direction. Axial load was defined as constant monotonic load applied at nodes corresponding to the locations of the prestressing cables on the wall. Fig. 10b) shows the predicted crack patterns and failure modes of the wall in VecTor2. Direction and relative size of the cracks, as well as the formation of a large horizontal crack at the base of the wall are effectively captured, as illustrated in the figure.

The analytical hysteresis curves are superimposed over the experimental curves in Fig. 10c) for better comparison. It can be observed that the backbone curve of the hysteresis graph was predicted very accurately. Rupture of reinforcement is also predicated accurately.

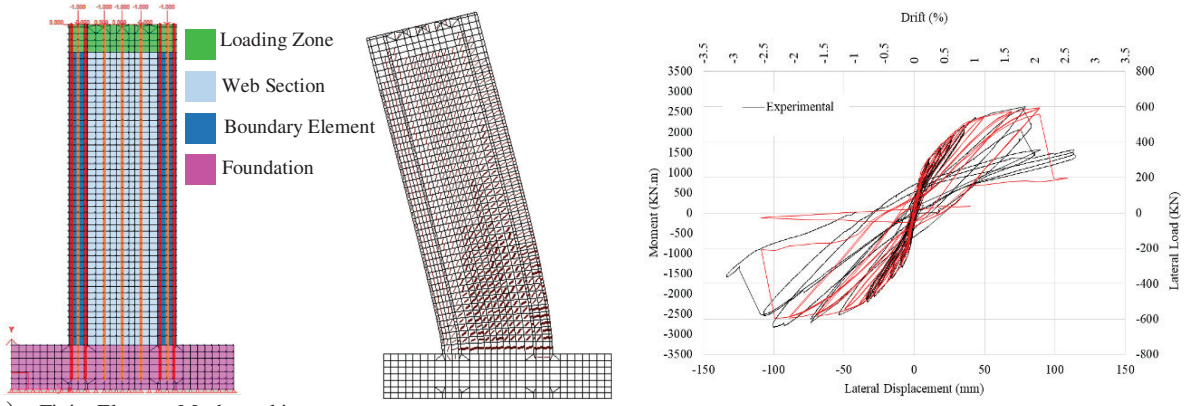

a) Finite Element Mesh used in VecTor2 Model

b) Modelled Cracking Pattern in VecTor2

c) Comparison of Wall W-2HS Experimental and Analytical Hysteretic Curves

Fig. 10 - Wall W-2HS FEM Model obtained using Vector2 Software

2.1 Parametric Study

An analytical parametric study was conducted using VecTor2 FEM software to investigate the effect of varying aspect ratio as well as the steel type on the behavior of the wall. Wall W-2HS was modelled using different height-to-length (H/L) aspect ratios and reinforcement types while all other wall parameters were kept the same as the tested wall specimen.

Fig. 11a) to d) show hysteretic curves for walls modelled with aspect ratios of 1.0, 2.0, 3.0, and 4.0. Increasing the wall`s aspect ratio does not appear to impact ductility of the wall in a consistent pattern. Ductility ratio of the wall with H/L = 2.0 is 4.4 which is the highest of the four modelled walls. The wall with H/L = 3.0 exhibits the lowest ductility ratio. The wall with an aspect ratio of 1.0 fails in shear and is unable to reach its ultimate moment capacity.

Fig. 11e), f), and g) show hysteretic curves for walls modelled with 400 MPa, 550 MPa, and 690 MPa reinforcement conforming to ASTM A615, ASTM A706, and ASTM A1035, respectively. Note that the longitudinal reinforcement ratios in the boundary elements of the modelled walls were adjusted in proportion to the yield strengths of corresponding reinforcement to match the probable moment resistance of the tested wall specimen. It can be seen that Grate 690 MPa reinforcement results in the least wall ductility. Slightly higher ductility is observed in the wall modelled with Grade 550 MPa. Wall modeled with Grade 400 MPa reinforcement has the highest ductility.

Analytically-obtained strain readings for the outermost boundary element longitudinal reinforcement for walls with different aspect ratios are plotted in Fig. 12. This plot suggests that as the aspect ratio of the wall increases, the spread of plasticity in the longitudinal flexural reinforcement along the height of the wall slightly decreases. Fig. 13 shows strain readings for the outermost boundary element longitudinal reinforcement for walls modelled with Grades 400 MPa, 550 MP and 690 MPa steel. It can be observed that the spread of plasticity in the flexural reinforcement is the smallest for Grade 690 MPa steel. Grade 550 MPa steel exhibits similar behaviour; however, Grade 400 steel shows significantly higher plasticity spread. This phenomenon can explain the different cracking patterns observed in the tested wall. As previously explained, cracks above the base of the wall do not widen significantly throughout the test. Only a horizontal crack at the base of the wall continues to widen and opens significantly closer to the ultimate load stage. Most of the plastic rotation occurs in the vicinity of this base crack as presented in Fig. 8.

The plasticity of the boundary element longitudinal reinforcement in Grades 690 MPa and 400 MPa extend to h/H = 0.1 (433mm) and h/H = 0.5 (2165mm), respectively. CSA A23.3-14 [4] specifies the minimum

plastic hinge regions in shear walls as $0.5l_w+0.1h_w$, where l_w is the length of the wall and h_w is the height of the wall. This is equal to 1158mm for wall W-2HS. Based on this observation, it may be prudent to evaluate plastic hinge length formulation for walls with higher strength reinforcement.

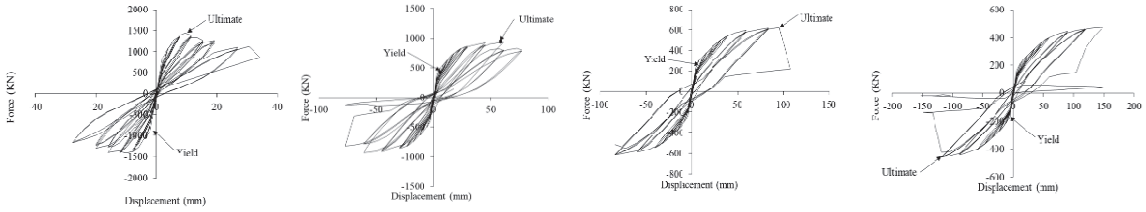

a) Wall W-2HS-1 H/L = 1.0

b) Wall W-2HS-2 H/L = 2.0

c) Wall W-2HS-3 H/L = 3.0

d) Wall W-2HS-4 H/L = 4.0

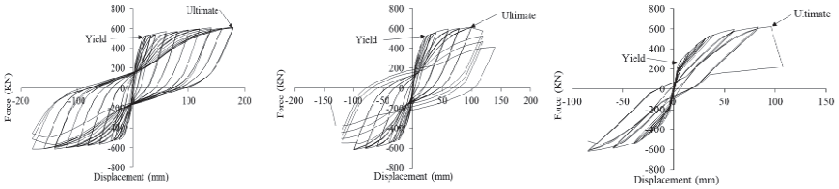

e) Wall W-2HS-5 f_y = 400 MPa (ASTM A615)

f) Wall W-2HS-6 f_y = 550 MPa (ASTM A706)

g) Wall W-2HS-7 f_y = 690 MPa (ASTM A1035)

Fig. 11 - Analytical Hysteretic Curves for Wall W-2HS with Varying Steel Type and Aspect Ratio (H/L)

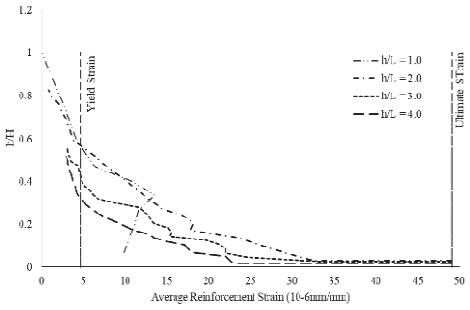

Fig. 12 Boundary element longitudinal reinforcement strains of walls modelled using different H/L aspect ratios

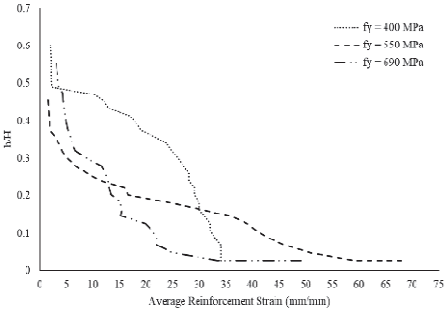

Fig. 13 - Boundary element longitudinal reinforcement strains of walls modelled using different H/L aspect ratios

Table 2 - Ductility and Energy Dissipation Capacity for Modelled Walls

Parameter	Wall Name	Energy Dissipated (KN.m)	Δ_y (mm)	Δ_u (mm)	μ
Aspect Ratio	AR4-FY690	52.6	48.0	148.0	3.1
	AR3-FY690	50.5	35.8	95.0	2.7
	AR2-FY690	91.7	17.7	77.1	4.4
	AR1-FY690	50.2	6.0	19.2	3.2
Steel Type	AR3 - FY400	184.0	23.9	179.0	7.5
	AR3 - FY550	147.9	15.9	119.6	7.5
	AR3 – FY690	50.5	35.8	95.0	2.7
	W-HS2 (Exp.)	44.6	38.7	89.2	2.3

Δ_y = yield displacement; Δ_u = ultimate displacement; μ = ductility ratio (Δ_u / Δ_y).

Table 2 presents energy dissipation capacity and ductility ratios for the modelled walls. While the effect of aspect ratio on the energy dissipation capacity of the walls may not follow a trend, it is clearly shown that walls reinforced with Grades 400 MPa and 550 MPa steel have significantly higher energy dissipation capacities. Proportionately, the ductility ratios of these walls are also higher than those reinforced with Grade 690 MPa steel. With higher ductility, the wall is allowed to undergo larger deformations resulting in additional cracking and crushing or concrete as well as reinforcement elongations which dissipate a considerable amount of energy.

6. Summary and Conclusions

A concrete shear wall reinforced with 690 MPa (ASTM A1035) steel bars was tested under combined reversed cyclic loading and constant axial load. The high-strength reinforcement used in this experiment did not have a defined yield point or yield plateau and had approximately 50% less ductility compared to conventional Grade 400 MPa (ASTM A615) reinforcing steel. The flexural reinforcement ratio of the tested wall was reduced in proportion to the ratio of the tensile strengths of 400 MPa to 690 MPa reinforcement and was detailed to produce the same probable moment of a control wall that was previously tested by Navidpour [10]. The control wall had identical geometry and was reinforced with conventional Grade 400 MPa reinforcement.

An analytical parametric study of the wall using different height-to-length aspect ratios as well as different reinforcing steel types was conducted using VecTor2 Finite Element Modelling Software

The findings of this study are summarized as follows:

1) Higher grade reinforcement such as Grade 690 MPa that lack a defined yield point and have smaller ductility ratio compared to conventional 400 MPa steel, may reduce ductility of reinforced concrete shear walls. It was observed that, while achieving similar flexural capacity, and similar hysteretic behaviour up to a drift level of 1.5%, wall W-2HS exhibited approximately 29% less ductility compared to the control wall.

2) Cracking pattern and plastic hinging behaviour in wall W-2HS appear to be different than those of the control wall. Unlike in walls reinforced with conventional 400 MPa steel where the plastic hinge rotation is spread out within the expected (prescribed) plastic hinge region, the majority of the plastic rotation within the design plastic hinge region of the tested wall occurred at the base of the wall where a large horizontal crack formed and continued to widen until the end of testing. It was analytically shown that plasticity of the flexural reinforcement was limited to approximately 250mm of the wall base ($0.06h_w$) where it increased drastically and resulted in bar rupture. Above this section, steel remained partially elastic. It is believed to be due to this behaviour that the cracks above the base of the wall maintained approximately the same width throughout the test and did not widen significantly. It may be prudent to evaluate current plastic hinge formulations for high-strength reinforcement; particularly those that do no exhibit conventional yield behaviour.

3) Shear deformations were found to be negligible throughout the test, as expected. This indicated that shear stresses were low and that the wall was adequately reinforced against shear.

4) A parametric study was conducted using VecTor2 FEM software. Wall W-2HS was modelled using different aspect ratios and reinforcing steel types. It was shown that the energy dissipation capacity and the ductility ratio of walls reinforced with Grade 400 MPa and 550 MPa steel are significantly higher compared to the wall reinforced with Grade 690 MPa steel. Steel type was found to have a significant impact on the plastic hinging behaviour of the wall, as described in conclusion #2 above. It was also shown that changing wall's aspect ratio from 1 to 4 does not impact the energy dissipation capacity or ductility of the wall in a discernable manner; however, it was noted that the wall with an aspect ratio of 2 exhibited the highest energy dissipation capacity and ductility ratio. Varying wall aspect ratio was also found to have little effect on plastic hinging behavior.

5) Current standards for seismic design of concrete structures lay out design requirements that are intended to achieve a minimum level of performance that is crucial for the integrity of a structure. This is often achieved via a series of prescriptive criteria on material properties, reinforcement detailing, stiffness, ductility, etc. Even though such specifications result in a demonstrably safe design, they often ignore the expected overall performance of the structure. This study demonstrates that Grade 690 MPa (ASTM A1035) reinforcement can reduce ductility of shear walls. In the case of wall W-2HS, this reduction is 29% compared to a wall constructed with conventional Grade 400 (ASTM A615) reinforcement. Even though the tested wall was designed to be a 'ductile wall' and that it failed the seismic performance criteria for such walls, it provided adequate ductility (2.0% drift) for a 'moderately ductile' wall. Such walls can be used in many areas around the world with moderate seismic design requirements (i.e. Ottawa, Canada). Considering its potential advantages, the use of high-strength reinforcement in seismic structures can significantly benefit the industry. Currently, further research is needed to identify and establish the necessary adjustments to current design specifications to allow for a performance-based approach in the design of seismic shear walls using high-strength reinforcement.

6. Acknowledgements

This project was funded by the Natural Sciences and Engineering Council of Canada (NSERC). The authors gratefully acknowledge the donations of materials from MMFX Technologies - a Commercial Metals company.

6. References

[1] ASTM, 2009a (2009): Standard Specification for Deformed and Plain Carbon-Steel Bars for Concrete Reinforcement, ASTM A615-09b. *ASTM International*, West Conshohocken, Pennsylvania.

[2] ASTM, 2009b (2009): Standard Specification for Low-Alloy Steel Deformed and Plain Bars for Concrete Reinforcement, ASTM A706-09b. *ASTM International*, West Conshohocken, Pennsylvania.

[3] ASTM, (2011): Standard Specification for Deformed and Plain, Low-Carbon, Chromium, Steel Bars for Concrete Reinforcement, ASTM A1035. *ASTM International*, West Conshohocken, Pennsylvania.

[4] ACI Committee 318 (2014): Building Code Requirements for Structural Concrete (ACI 318-14) and Commentary (ACI 318R-14). *American Concrete Institute*, Farmington Hills, MI, 519 pp.

[5] Baek, J.W., Park, H.G., Lee, J.H. and Bang, C.J., (2017): Cyclic loading test for walls of aspect ratio 1.0 and 0.5 with grade 550 MPa (80 ksi) shear reinforcing bars. *ACI Structural Journal*, 114(4), p.969.

[6] Cheng, M.Y.; Hung, S.C.; Lequesne, R.D.; Lepage, A. (2016): Earthquake-Resistant Squat Walls Reinforced with High-Strength Steel. *American Concrete Institute Structural Journal*, 113(5), 2016, pp.1065-1076.

[7] CSA A23.3-14: Design of Concrete Structures (2014): *Canadian Standards Association, Mississauga*, Canada.

[8] Dazio, A.D.A., Beyer, K., and Bachmann, H. (2009): Quasi-static cyclic tests and plastic hinge analysis of RC structural walls. *Engineering Structures*, Vol. 31, pp. 1556-1571.

[9] Kimura, H. and Ishikawa, Y. (2008): Seismic Performance of High-Strength Reinforced Concrete Slender Walls Subjected to High Axial Loading. *8th International Symposium on Utilization of High-Strength and High-Performance Concrete*, Tokyo, Japan, Oct. 27-29, S1-4- 4, 945-950.

[10] Navidpour, M. (2018): Reinforced Concrete Shear Walls with Welded Wire Grids as Boundary Element Transverse Reinforcement (Doctoral Dissertation). University of Ottawa, Ottawa, ON.

[11] NIST GCR 14-917-30 (2014): Use of High-Strength Reinforcement in Earthquake-Resistant Concrete Structures. *NEHRP Consultants Joint Venture*, Gaithersburg, MD, 231 pp.

[12] Suzuki, T., Laughery, L. and Pujol, S. (2018): Learning from the Japanese Experience with High-Strength Longitudinal Reinforcement. *Concrete International*, 40(9), pp.47-58.

[13] Sokoli, D., and Ghannoum, W. M. (2016): High-Strength Reinforcement in Columns under High Shear Stresses. *ACI Structural Journal*. V. 113, No. 3, pp. 605-614.

